Astronomy & Astrophysics manuscript no. GMCep
May 23, 2018

On the nature of the variable young star GM Cep

T. Giannini[1], U. Munari[2], D. Lorenzetti[1], S. Antoniucci[1], F. Castellani[3], D. Dallaporta[3], R. Jurdana-Šepić[4]

[1] INAF - Osservatorio Astronomico di Roma - Via Frascati, 33 - Monte Porzio Catone 00078, Italy
[2] INAF - Osservatorio Astronomico di Padova - via dell'Osservatorio 8, Asiago (VI) 36012, Italy
[3] ANS Collaboration, Astronomical Observatory, 36012, Asiago (VI), Italy
[4] Physics Department, University of Rijeka, Radmile Matčič, 51000 Rijeka, Croatia

Received date / Accepted date

ABSTRACT

Context. GM Cep is a young Pre-Main Sequence source that presents rapid photometric variability of more than 2 mag in the optical bands. First studies have interpreted such variations as possible EXor-type outbursts, but subsequently important arguments in favour of a quasi-periodical UXor-type variability have been provided.
Aims. We aim to get significant insights on the origin of the variability of GM Cep by directly measuring the mass accretion rate onto the star in different brightness phases.
Methods. Optical BVR_CI_C photometry and low- and high-resolution spectroscopy were obtained between November 2017 and April 2018, a period during which GM Cep underwent a brightness increase from $V \sim 14.8$ to ~ 13.3 mag between November and March, then followed by a new fading at the end of April. The extinction toward the source was determined from color-color diagrams, while the mass accretion rate was derived from the Hα absolute flux.
Results. The average mass accretion rate is $(3.5 \pm 0.6)\times10^{-8}$ $M_\odot$ yr^{-1} . We do not find significant variations of this value with the increase of the source brightness, and therefore conclude that GM Cep did not experience any outbursting accretion event during our monitoring period.

Key words. Stars: pre-main sequence – Stars: variables: Tauri, Herbig Ae/Be – Stars: variables: general – Stars: individual: GM Cep

1. Introduction

An intense activity, in terms of strong brightness fluctuations, is a defining feature of the large majority of all the Pre-Main Sequence (PMS) stars. Among them, low mass objects are the best studied, since it is possible to investigate large samples of targets at the shortest distances. Large amplitude variability (2 to 5 mag), characterized by bursting and fading events from months to years timescales, is typically associated with two classes of young objects: EXors (Herbig 1989) and UXors (Grinin 1988). FUors (Hartmann & Kenyon 1985) belong to a third class of objects that do not offer any chance to investigate the intermittent variability, since they undergo a unique and strong outburst and then remain at this high level of luminosity for decades or centuries. Conversely, EXors and UXors are very suitable to unravel their fluctuation modalities. In essence, the objects whose variabilily is due to intermittent disk accretion events are classified as EXors; whereas, if the fluctuations are driven by a variable extinction along the line of sight (e.g. obscuration by an orbiting obstacle, evaporation/condesation of interveining dust, ejected material by powerful outflows), they are considered as UXors. However, many young variables obey to both mechanisms, whose mutual prevalence depends on the level of activity (Kun et al. 2011; Hillenbrand et al. 2013; Kóspál et al. 2016; Giannini et al. 2018). Hence, it is becoming clearer and clearer that, more than to merely classify an object as EXor or UXor, it is crucial to infer on the variation of its physical parameters, such as the rising/declining time of the fluctuations, their amplitude and cadence, the mass accretion/loss rate, the time dependence of visual extinction A_V, the phenomena timescale, and, more importantly, the possible existence of (inter-)relationships between accretion and extiction events. Indeed, both these events have important implications for planet evolution: disk accretion has naturally a finite lifetime that gives constraints on the timescale of planet formation (Hartmann, Herczeg & Calvet, 2016); while extinction by dust aggregated along the line of sight is likely related to occultation by proto-planetary clumps (Chen et al. 2012). Since theoretical models able to provide quantitative predictions of the observed phenomena do not exist at the moment, the problem has to be attacked observationally, by accurately monitoring suitable targets both photometrically and spectroscopically in a range of frequencies as wide as possible.
To this scope we have recently undertaken an optical monitoring of the source GM Cep. This is a Pre-Main Sequence variable ($M \sim 2.1$ $M_\odot$, spectral type G7V-K0V - Sicilia-Aguilar et al. 2008) in the young open cluster Trumpler 37, at a distance of 825±18 pc (Gaia DR2[1]). During the recent decade, GM Cep has been well studied in a wide wavelength range. Sicilia-Aguilar et al. (2008) interpreted its variability as the result of episodic disk accretion events (EXor-type); the presence of a massive disk was confirmed by Herschel observations (Sicilia-Aguilar et al. 2015). Conversely, Xiao, Kroll, & Henden (2010) showed a historical light-curve dominated by recurrent fading, interpreted as eclipse events (UXor-type). Brightness drops with a recurrence timescale of about one year was evidenced by Chen et al. (2012), who interpreted them as an obscurarion of the central star by orbiting dust concentrations. The same conclusion has

Send offprint requests to: Teresa Giannini, e-mail: teresa.giannini@oa-roma.inaf.it

[1] http://gea.esac.esa.int/archive/

been reached by Semkov & Peneva (2012) and, more recently, by Semkov et al. (2015), who observed also high amplitude rapid variations typical of active T Tauri stars. Huang et al. (2018) observed a variable polarization of GM Cep (from 3 to 9%), whose level is anticorrelated with the source brightness, likely indicating light scattering by dust clumps.

Optical spectra of the source were taken by Sicilia-Aguilar et al. (2008) and Semkov et al. (2015), both obtained when the source was close to its maximum luminosity. However, GM Cep was never sampled by taking simultaneous photometry and spectroscopy. In this paper we start to fill this gap, presenting observations obtained between late 2017 and early 2018, a period during which GM Cep underwent a visual brightness variation of nearly two magnitudes. Our recent observations are presented in Sect.2; the results are analysed in Sect.3, while concluding remarks are given in Sect.4.

2. Observations

After publishing our telegram (Munari et al. 2017) to announce a sudden decrease of brightness, we have undertaken a tight photometric and spectroscopic monitoring of GM Cep. We present here the results collected in this campaign from 30 November 2017 until 25 April 2018. Although being relatively short for inferring on the GM Cep epocal behaviour, our monitoring is significant to derive important features of the light curve. Archival data of plates photometry covering a period between 1961 and 1968 are also given to provide additional information on the photemetric variability.

2.1. Optical photometry

BVR_CI_C optical photometry (Table 1) has been obtained with telescopes ID 31 and ID 66 operated in Cembra and Mt. Baldo (Italy) by the Asiago Novae and Symbiotic stars (ANS) Collaboration. Raw data were treated for nightly bias, dark and flat fields in a standard manner. The transformation from the local istantaneous system to the standard one (Landolt) was achieved via color-equations calibrated on a local photometric sequence extracted from the the APASS survey data (Henden et al. 2012, Henden & Munari 2014), and ported to the Landolt's system of equatorial standards via the transformation equations calibrated in Munari et al. (2014).

2.2. Archival plates

All the details of our plates observations (operated Schmidt telescopes, filters and exposition times) are given in our papers explicitly devoted to plate analysis (Jurdana-Šepić, et al. 2017, 2018). Here we remind that two Schmidt telescopes were operated at the Asiago Astronomical Observatory. The smaller telescope (SP, 40/50 cm, 100 cm focal length) observed between 1958 and 1992, with photographic films. The larger telescope (SG, 67/92 cm, 208 cm focal length) observed with square glass photographic plates (5°×5°) between 1965 and 1998, after which large format CCDs were used as detectors. Nearly all plates from both telescopes go very deep, $B\sim18.5$ and $B\sim17.8$ mag being the typical limiting magnitude for blue sensitive plates exposed with the SG and SP telescopes, respectively.

The Asiago plates cover an uninterrupted interval of 40 years, and are accurately preserved in a controlled environment. A total of 31 plates were found to image GM Cep, covering a period of about 8 yrs (from 1961 January to 1968 November) The resulting magnitudes (approximately B and V bands) are listed in Table 2.

2.3. Optical spectroscopy

Table 3 gives the journal of the spectroscopic observations. During our monitoring period we obtained 13 spectra of GM Cep. Out of these, seven were acquired in the low-resolution modality with the 1.22m telescope + B&C spectrograph operated in Asiago by the University of Padova. These spectra cover the wavelength range between 3300 and 8050 Å at $\Re \sim 2400$. The slit has been kept fixed at a width of 2″, and always aligned with the parallactic angle for optimal absolute flux calibration. In addition, six high-resolution optical spectra at $\Re \sim 18\,000$, spectral range 3300−8050 Å , were acquired with the REOSC Echelle spectrograph mounted on the Asiago 1.82 m telescope. The integration time is 1 hr for both low- and high-resolution spectra.

Steps of the data reduction are the same for both low- and high-resolution spectra: each two-dimensional spectral image was first corrected for dark and bias frames and then flat-fielded. The one-dimensional spectrum was extracted by integrating the stellar trace along the spatial direction. The sky background was traced on both sides of GM Cep spectrum and subtracted to it. Wavelength calibration was obtained from the spectra of arc lamps (FeHeAr and Thorium), while flux calibration was achieved against nightly observations of red standard stars. The zero-point of the flux scale was then checked against the flux integrated through the Landolt V pass-band and the photometric V magnitude.

3. Results and analysis

3.1. Light curve and photometric diagrams

The light curve of GM Cep was derived from observations taken with two independent telescopes (Figure 1, data depicted with different symbols). Noticeably, the two measurements are in perfect agreement, since they are consistent even in tracing the smallest photometric variations of few cents of magnitude. Between November and March, GM Cep presented a continuous and slow trend of increasing brightness in all bands, whose amplitude is of about 2.5 mag in B, 1.5 mag in V and 1 mag in R and I. Then the source has started a new fading phase. On monthly timescale and superimposed to this trend, are intermittent variations of amplitude up to 1 mag, and rising/declining times of about 20/10 days. The peak-to-peak brightness variation is smaller than that (2-2.5 mag in V) previously monitored by different authors (e.g. Sicilia-Aguilar et al. 2008; Semkov et al. 2015). Reasonably, this is a mere consequence of our shorter monitoring period (about 150 days vs. few years), during which the probability to detect larger fluctuations is clearly reduced. All the colors (upper panels of Figure 1) become bluer whenever the brightness increases. This behaviour is suggestive of extinction-driven fluctuations, but also accretion events often show the same effect, since they provoke a sudden increase of the luminosity due to the appearance of an excess continuum emission at short (UV-blue) wavelengths associated with the accretion shock. In the following, we try to solve this degeneracy which is inherent to any purely photometric analysis. A complementary insight into the color analysis is illustrated in Figure 2. The left and middle panels depict the col-col plots $[V-R]$ vs. $[B-V]$ and $[R-I]$ vs. $[V-R]$, while the col-mag plot $[V-I]$ vs. $[V]$ is presented in the right panel. Red (black) symbols represent the cases when the source was brighter (fainter) than 14.5

Table 1. Optical photometry.

Tel .	HJD	Date	B	V	R_C	I_C	$[B-V]$	$[V-R_C]$	$[R_C-I_C]$
66	2458081.30912	2017 11 23.809	16.259	14.691	13.955	12.948	1.540	0.923	1.926
66	2458084.29522	2017 11 26.795	16.444	14.862	14.015	13.079	1.573	0.974	1.960
66	2458085.29266	2017 11 27.793	16.337	14.808	13.905	12.979	1.547	0.988	1.929
66	2458088.30608	2017 11 30.806	16.369	14.836	13.844	12.856	1.573	1.011	1.978
31	2458088.33736	2017 11 30.837	16.391	14.856	13.880	12.895	1.530	0.961	1.953
31	2458091.29664	2017 12 03.797	.....	14.993	13.975	12.964	.....	0.996	2.020
66	2458091.32967	2017 12 03.830	16.529	15.000	13.986	12.967	1.530	1.040	2.040
66	2458093.27799	2017 12 05.778	16.473	14.862	13.870	12.838	1.574	0.991	2.003
31	2458093.30257	2017 12 05.803	16.434	14.871	13.846	12.810	1.542	1.022	2.063
66	2458094.31080	2017 12 06.811	16.376	14.795	13.783	12.752	1.566	1.003	2.016
66	2458095.27392	2017 12 07.774	16.446	14.884	13.859	12.843	1.532	1.005	2.006
31	2458097.26316	2017 12 09.763	16.348	14.779	13.775	12.732	1.551	0.985	2.034
66	2458097.32672	2017 12 09.827	16.372	14.799	13.776	12.745	1.549	1.007	2.021
66	2458100.45815	2017 12 12.958	16.199	14.589	13.588	12.574	1.545	0.985	1.991
66	2458103.25964	2017 12 15.760	16.194	14.711	13.714	12.675	1.561	0.983	1.981
31	2458103.31946	2017 12 15.819	.....	14.638	13.635	12.637	.....	0.981	1.983
66	2458104.29517	2017 12 16.795	15.932	14.330	13.371	12.421	1.558	0.961	1.893
66	2458105.26002	2017 12 17.760	15.658	14.099	13.182	12.264	1.563	0.920	1.823
31	2458106.27320	2017 12 18.773	15.732	14.190	13.259	12.358	1.533	0.914	1.828
66	2458106.31830	2017 12 18.818	15.738	14.186	13.265	12.347	1.556	0.923	1.823
66	2458108.37425	2017 12 20.874	15.738	14.190	13.296	12.373	1.528	0.888	1.795
31	2458110.26241	2017 12 22.762	15.623	14.127	13.220	12.329	1.484	0.895	1.795
66	2458110.34165	2017 12 22.842	15.648	14.118	13.228	12.327	1.503	0.877	1.762
66	2458112.25830	2017 12 24.758	15.659	14.128	13.225	12.312	1.513	0.891	1.785
31	2458113.27672	2017 12 25.777	15.545	14.020	13.111	12.220	1.521	0.899	1.795
66	2458113.32909	2017 12 25.829	15.580	14.024	13.124	12.228	1.555	0.879	1.771
31	2458118.21074	2017 12 30.711	.....	14.464	13.490	12.527	.....	0.958	1.920
66	2458118.30978	2017 12 30.810	15.923	14.428	13.473	12.530	1.480	0.935	1.864
66	2458120.30777	2018 01 01.808	16.107	14.632	13.688	12.715	1.455	0.925	1.855
31	2458121.25904	2018 01 02.759	16.139	14.651	13.710	12.729	1.525	0.932	1.913
66	2458121.33991	2018 01 02.840	16.179	14.675	13.737	12.766	1.529	0.908	1.880
31	2458131.29853	2018 01 12.799	15.924	14.368	13.383	12.420	1.556	0.975	1.939
66	2458131.35199	2018 01 12.852	15.909	14.349	13.373	12.402	1.538	0.961	1.917
66	2458132.35528	2018 01 13.855	15.809	14.219	13.250	12.323	1.570	0.948	1.762
66	2458135.32786	2018 01 16.828	15.187	13.681	12.806	11.965	1.503	0.861	1.681
31	2458137.27379	2018 01 18.774	15.226	13.742	12.870	12.015	1.492	0.870	1.727
66	2458137.35554	2018 01 18.856	15.203	13.713	12.846	11.878	1.492	0.848	1.710
66	2458138.35243	2018 01 19.852	15.299	13.818	12.926	12.017	1.452	0.874	1.742
66	2458140.29900	2018 01 21.799	15.258	13.778	12.889	12.094	1.474	0.871	1.748
31	2458142.23991	2018 01 23.740	15.600	14.088	13.148	12.247	1.519	0.930	1.829
66	2458142.31192	2018 01 23.812	15.638	14.102	13.176	12.207	1.516	0.910	1.829
31	2458146.23726	2018 01 27.737	15.585	14.024	13.076	12.145	1.557	0.943	1.868
66	2458146.33166	2018 01 27.832	15.614	14.038	13.089	12.161	1.539	0.929	1.869
66	2458147.28929	2018 01 28.789	15.409	13.930	12.976	12.053	1.467	0.919	1.807
66	2458149.29630	2018 01 30.796	15.180	13.712	12.827	11.949	1.490	0.861	1.733
31	2458153.25833	2018 02 03.758	14.884	13.464	12.620	11.817	1.420	0.834	1.640
31	2458160.26944	2018 02 10.769	14.787	13.390	12.569	11.783	1.417	0.810	1.607
66	2458160.40154	2018 02 10.902	14.826	13.442	12.625	11.820	1.382	0.804	1.636
66	2458161.27437	2018 02 11.774	14.944	13.479	12.655	11.835	1.410	0.808	1.621
31	2458164.29755	2018 02 14.798	.....	13.444	12.622	11.814	.....	0.807	1.625
31	2458166.25110	2018 02 16.751	14.704	13.324	12.545	11.732	1.466	0.769	1.595
31	2458175.70036	2018 02 26.200	.....	13.810	12.884	11.980	.....	0.926	1.833
31	2458185.65821	2018 03 08.158	15.025	13.555	12.701	11.900	1.510	0.871	1.725
66	2458191.64153	2018 03 14.142	14.771	13.354	12.514	11.704	1.366	0.832	1.627
66	2458210.60454	2018 04 02.105	15.075	13.664	12.806	11.920	1.354	0.844	1.729
31	2458214.55729	2018 04 06.057	15.139	13.795	12.926	12.067	1.388	0.872	1.728
66	2458222.55523	2018 04 14.055	15.114	13.770	12.932	12.073	1.288	0.826	1.673
66	2458227.61789	2018 04 19.118	15.277	13.954	13.123	12.246	1.285	0.828	1.688
31	2458228.57948	2018 04 20.079	15.397	14.143	13.333	12.475	1.275	0.804	1.664
66	2458233.53681	2018 04 25.037	15.006	13.575	12.717	11.851	1.371	0.842	1.705

Notes. Errors on magnitudes are less than 0.02 mag.

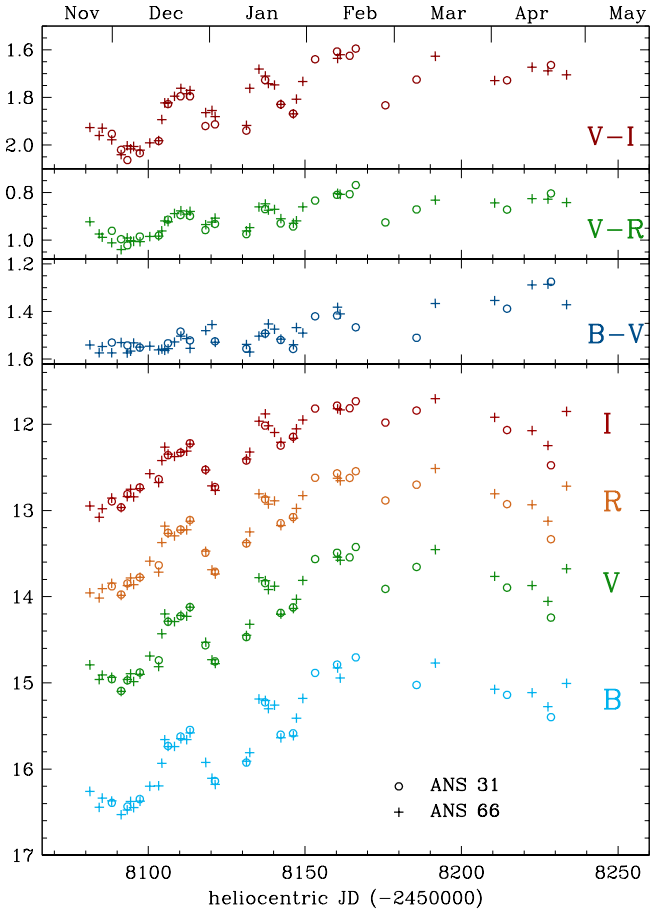

Fig. 1. *BVRI* lightcuves (bottom panel) and colors (upper panels) of GM Cep obtained during the recent period of activity. Crosses/circles refer to the data taken with telescope 66 and 31, respectively.

V-mag. In both color the data align along the extinction vector (reddening law of Cardelli et al. 1989). In both cases, the average A_V toward the source is $\simeq$ 2.5 magnitudes, while an extinction variability of $\Delta A_V \simeq 0.8$ and 1.2 mag are derived from the left and middle plot, respectively. Noticeably, the slight difference between the two determinations can be reconciled by assuming that the color $[B - V]$ is squeezed to smaller values owing to a B-band excess due to a significant mass accretion rate typical of PMS stars (although such effect is mainly evident in the U-band). The col-mag plot indicates a good alignment of the data points with the extinction vector until the source is in a bright state (red points). For fainter magnitudes, however, a color reversal becomes evident (black points). This is a well known effect (so-called 'blueing effect') that is a typical feature of UXor-type sources (e.g Bibo & The 1990; Grinin et al. 1994), which becomes observable when the obscuration is high enough to make the fraction of light scattered by small dust grains significant.

3.2. Comments on archival plates

With reference to the archival light curve of Figure 3, we note that a meaningful number of detections has been obtained only in the V band (lower panel). The very few B-band measurements (upper panel) are plotted just to have a quick comparison with the observational periods investigated by Xiao et al. (2010) by means of plate photometry (green points). Remarkably, our data cover a complementary period, filling a gap of about six years in the Xiao et al. record. The fluctuations retrivable from our V-band photometry present a total amplitude of a couple of magnitudes, in agreement with both the results and modalities suggested by more recent long term monitoring programs (Sicilia-Aguilar et al. 2008; Semkov et al. 2015). This occurrence is a futher confirmation that our historical data do not contraddict the UXor nature of GM Cep. Unfortunately, a color analysis cannot be attempted either with our own data, or combining them (V band) with those by Xiao et al., whose B-band photometry does not cover our time interval.

3.3. Spectroscopy

3.3.1. Low-resolution

The low-resolution spectra of GM Cep are shown in Figure 4. These provide further hints in favour of an UXor-type variability of GM Cep. These are briefly summarized here. 1) The slope of the UV part of the spectrum does not decrease from the low to the bright state, but rather it slightly increases. This is contrary to what expected in case of an enhancement of the accretion rate, which is usually associated with an increase of the Balmer continuum emission at wavelengths shorter than 365 nm (e.g.

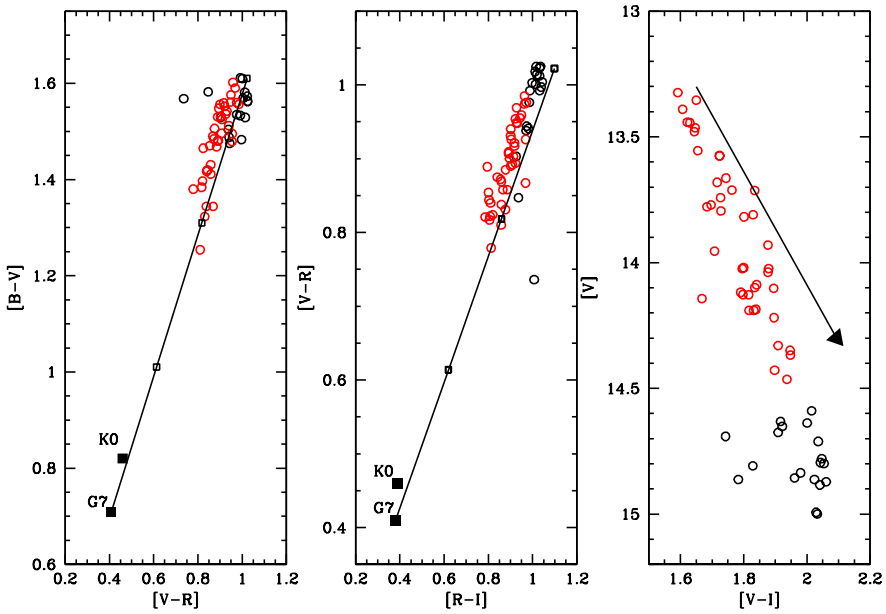

Fig. 2. Left panel: $[V-R]$ vs. $[B-V]$ plot. Black and red data points correspond to $V >$ and ≤ 14.5 mag, respectively. The black line shows the extinction vector direction (according to the reddening law of Cardelli et al. 1989). Filled squares give the colors of an un-reddened G7 and K0 main-sequence star, while open squares indicate an extinction increase of 1 mag. Middle panel: $[R-I]$ vs. $[V-R]$ plot. Symbols have the same meaning as in the left panel. Right panel $[V-I]$ vs. $[V]$ plot. The arrow shows the extinction vector direction. Other symbols as in the left panel.

Valenti et al. 1993; Gullbring et al. 1998; Herczeg & Hillenbrand 2008; Rigliaco et al. 2012). 2) Apart from a bright Hα line, no other spectral feauture is in emission, while Hβ is seen in absoprtion in the spectra of 2018 January 28 and 2018 February 14. The same is seen in the spectra of 2001 July and 2007 April, during two phases of maximum (Sicilia-Aguilar et al. 2008). Typically, accreting protostars present the hydrogen recombination lines in emission, and with similar profiles (e.g. Muzerolle, Calvet, & Hartman 2001). Conversely, Hβ in absoprtion is a defining feature of UX Ori type stars (Grinin et al. 2001). 3) The equivalent width of the photospheric lines (detected in almost all spectra, although with a low signal-to-noise ratio in the faintest ones) remains roughly constant at the different dates. This is what expected in case of variable extinction, because this influences in the same way both lines and overlying continuum. Conversely, in case of an enhancement of the accretion rate, the photospheric lines should be veiled when the source is bright, because of the excess emission produced by the hot spot(s) on the stellar surface.

3.3.2. High resolution Spectroscopy

Here we briefly comment on the kinematical evolution of the Hα and Hβ profiles during our monitoring period. The Hα profile (Figure 5) was deconvolved in two or three Gaussians using the curve-fitting tool *splot* inside the IRAF[2] package, whose parameters are given in Table 4. In the first three dates, the profile is deconvolved in a main component, slightly red-shifted (with respect to the heliocentric coordinates), FWHM $\sim$ 250 km s^{-1} and EW $\sim$ between 400 and 600Å , plus a narrower blue-shifted component, centered around $-$ 200 km s^{-1} and FHWM $\sim$ 150 km s^{-1}. In the last three dates, the Hα profile appears more complex, presenting signatures of self-absorption in the main component (that is fitted with two Gaussians) and a P-Cygni profile at about -100 km s^{-1}. This analysis of the Hα profile suggests two main considerations: 1) the line brigthness enhancement roughly follows that of the continuum, since the EW does not change significantly, and 2) the P-Cyg absorption is likely a signature of an outflowing wind (e.g. Edwards et al. 2003). This hypothesis is also reinforced by a rough detection of [O I] 6300Å emission, although centered at a slower speed of about -65 km s^{-1}.

The Hβ profile (Figure 6), as already evidenced in the low-resolution spectra, is seen in absorption with the exception of the spectrum of 2017 November 30. The line is dectected with a poor signal-to-noise ratio, and any attempt to fit the profile with a Gaussian function has given a negative result. We empirically estimate the line center at around -90 km s^{-1}, in good agreeemnt with the P-Cygni component of the Hα.

3.4. Mass accretion rate

A powerful way to determine whether or not GM Cep is an eruptive variable is to evaluate the variation of the mass accretion

[2] IRAF is the Image Reduction and Analysis Facility, a general purpose software system for the reduction and analysis of astronomical data. IRAF is written and supported by the National Optical Astronomy Observatories (NOAO) in Tucson, Arizona.

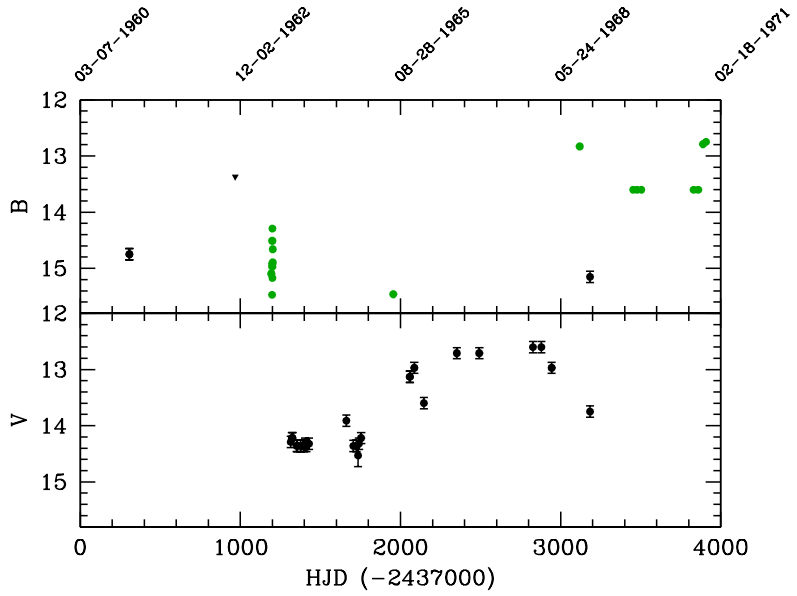

Fig. 3. *BV* plates light curves (black dots). *B* photometry by Xiao et al. (2010) between 1962 and 1971 is shown for comparison (green dots).

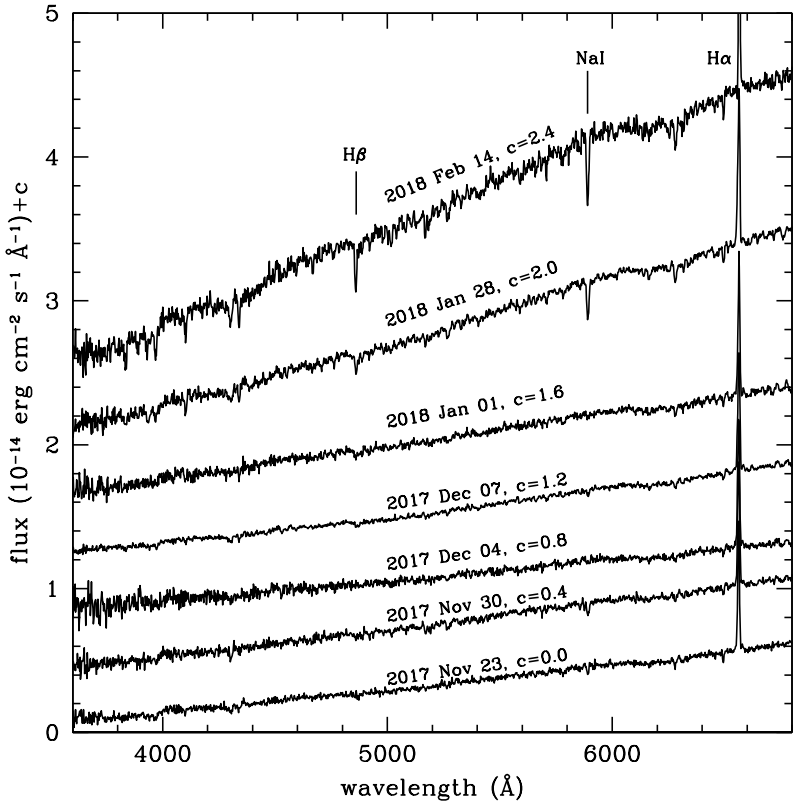

Fig. 4. Low-resolution spectra of GM Cep.

rate ($\dot{M}_{acc}$) between low- and high-brightness phases. The computation of $\dot{M}_{acc}$ is based on empirical relationships between the accretion luminosity ($L_{\rm acc}$) and the luminosity of selected emission lines. The relation between the Hα luminosity ($L_{H\alpha}$) and $L_{\rm acc}$ has been derived by Alcalá et el. (2017):

$$log(L_{\rm acc}/L_{\odot}) = (1.13 \pm 0.05)\, L_{H\alpha} + (1.74 \pm 0.19)\,, \quad (1)$$

$L_{\rm acc}$ can then been converted in $\dot{M}_{acc}$ through the relation by Gullbring at al. (1998):

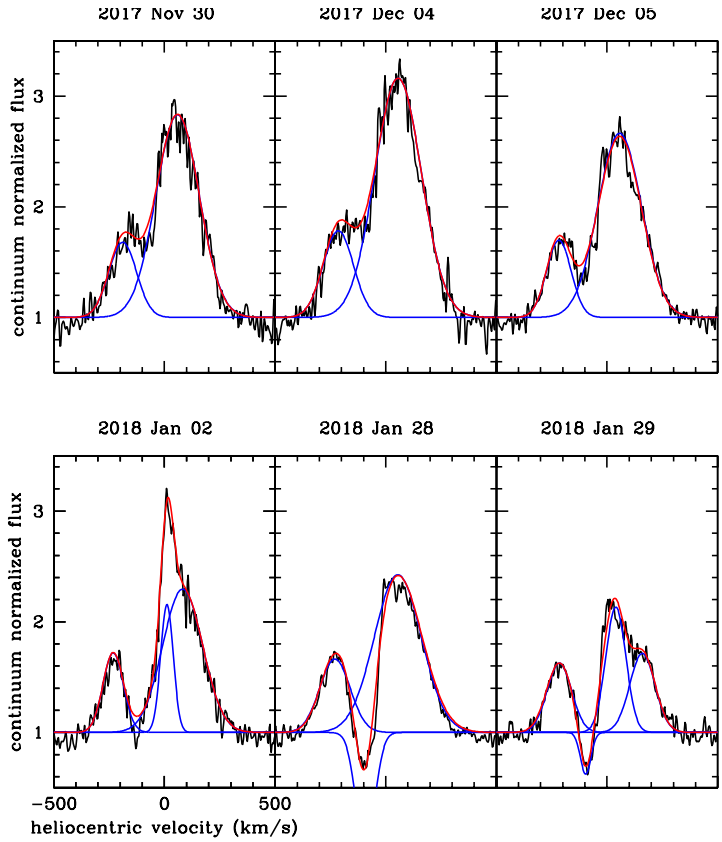

Fig. 5. Hα continuum-normalized profile (black) in different dates. In red we show the fit to the profile, obtained by adding multiple Gaussians (blue).

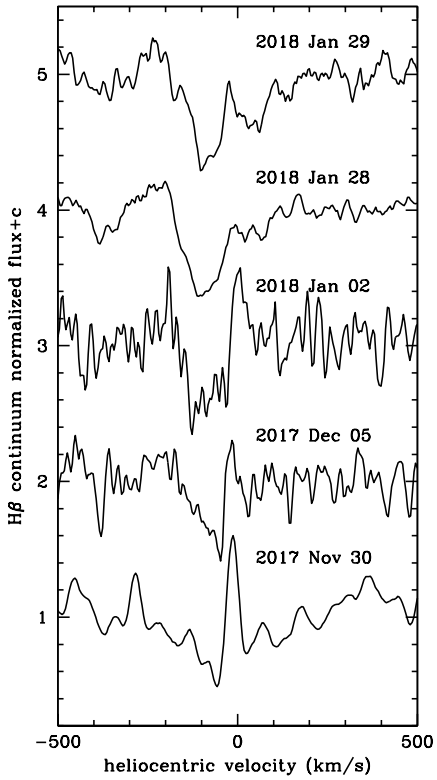

Fig. 6. Hβ continuum-normalized profile in different dates.

Table 2. Plate photometry. Columns provide: date and center UT of exposure, plate emulsion, adopted filter, plate number and magnitude. The estimated error is of 0.10 mag.

HJD	Date	UT	Emulsion	Filter	Plate	Mag
2437307.22037	1961 01 07	17:18	103 aO	LIQ	01259	B=14.75
2437307.23495	1961 01 07	17:39	103 aO	LIQ	01260	B=14.75
2437968.28065	1962 10 30	18:41	103 a-O	LIQ	03262	B>13.37
2438315.32609	1963 10 12	19:46	PANROY	—-	04118	V*=14.29
2438315.34484	1963 10 12	20:13	103 aE	RG1	04119	R=13.40
2438322.28086	1963 10 19	18:41	PANROY	—-	04164	V*=14.22
2438326.38218	1963 10 23	21:07	PANROY	—-	04195	V*=14.22
2438351.37389	1963 11 17	20:56	PANROY	—-	04241	V*=14.36
2438356.37303	1963 11 22	20:55	PANROY	—-	04269	V*=14.36
2438376.23543	1963 12 12	17:38	PANROY	—-	04310	V*=14.36
2438399.22123	1964 01 04	17:19	PANROY	—-	04384	V*=14.36
2438404.21615	1964 01 09	17:12	PANROY	—-	04445	V*=14.32
2438413.22826	1964 01 18	17:30	PANROY	—-	04508	V*=14.36
2438428.23810	1964 02 02	17:45	PANROY	—-	04563	V*=14.32
2438662.27615	1964 09 23	18:34	PANROY	—-	04880	V*=13.91
2438705.26660	1964 11 05	18:21	PANROY	—-	04957	V*=14.36
2438725.23123	1964 11 25	17:31	PANROY	—-	04982	V*=14.36
2438735.22389	1964 12 05	17:21	PANROY	—-	05024	V*=14.53
2438740.45145	1964 12 10	22:49	PANROY	—-	05109	V*=14.32
2438754.28001	1964 12 24	18:43	PANROY	—-	05136	V*=14.22
2439057.34676	1965 10 23	20:16	PANROY	—-	05588	V*=13.13
2439059.28561	1965 10 25	18:48	PANROY	—-	05606	V*=13.13
2439086.24041	1965 11 21	17:44	PANROY	—-	05634	V*=12.97
2439146.24552	1966 01 20	17:55	PANROY	—-	05712	V*=13.60
2439351.40457	1966 08 13	21:40	PANROY	—-	05972	V*=12.71
2439492.26371	1967 01 01	18:20	PANROY	—-	06192	V*=12.71
2439827.25529	1967 12 02	18:06	PANROY	—-	06457	V*=12.60
2439879.28222	1968 01 23	18:48	PANROY	—-	06532	V*=12.60
2439944.63983	1968 03 28	27:25	PANROY	—-	06704	V*=12.97
2440183.39244	1968 11 22	21:23	PANROY	—-	06941	V*=13.75
2440183.40216	1968 11 22	21:37	103 a-O	—-	06942	B=15.15

Table 3. Journal of the spectroscopic observations.

MJD	Date (yyyy mm dd)	Instr/Tel	$\Re$
58080	2017 11 23	B&C/1.22m	2400
58087	2017 11 30	B&C/1.22m	2400
58087	2017 11 30	ECH/1.82m	18 000
58091	2017 12 04	B&C/1.22m	2400
58091	2017 12 04	ECH/1.82m	18 000
58092	2017 12 05	ECH/1.82m	18 000
58094	2017 12 07	B&C/1.22m	2400
58119	2018 01 01	B&C/1.22m	2400
58120	2018 01 02	ECH/1.82m	18 000
58146	2018 01 28	B&C/1.22m	2400
58146	2018 01 28	ECH/1.82m	18 000
58147	2018 01 29	ECH/1.82m	18 000
58163	2018 02 14	B&C/1.22m	2400

$$\dot{M}_{acc}/\mathrm{M}_\odot\,\mathrm{yr}^{-1} = \frac{L_{acc}R_*}{GM_*}\left(1-\frac{R_*}{R_{in}}\right)^{-1} \quad , \tag{2}$$

Equations 1 and 2 have been applied considering a distance of 825 pc, a stellar mass $M_* = 2.1\,\mathrm{M}_\odot$, a radius $R_* = 3\,\mathrm{R}_\odot$, and an inner disk radius $R_{in} = 5R_*$. The Hα intrinsic flux at the different dates was computed by dereddening the observed flux for $A_V = 2.5$ mag, as derived by the color-color diagrams of Figure 2.

In Figure 7 we plot our results (black data points). No significant enhancement of the mass accretion rate can be evidenced, being all the determinations consistent inside the errorbars. These latter take into account both the uncertainty in the flux measurement and that in the $L_{\rm acc}$ vs. $L_{H\alpha}$ relationship. The average $\dot{M}_{acc}$ value is $(3.5 \pm 0.6)\times10^{-8}\,\mathrm{M}_\odot\,\mathrm{yr}^{-1}$, which is lower both than the determination of Semkov et al. (2015) of $18\times10^{-8}\,\mathrm{M}_\odot\,\mathrm{yr}^{-1}$ and than the range estimated by Sicilia-Aguilar et al. (2008) between 5 and $30\times10^{-8}\,\mathrm{M}_\odot\,\mathrm{yr}^{-1}$. At the time of both these observations, however, GM Cep was close to its maximum level of brigtheness, being $V \sim 12.9$ mag on June 2008 (Semkov et al. 2015) and $R \sim 12.9$ mag on June 2001 (Sicilia-Aguilar et al. 2008).

Both these authors have derived $\dot{M}_{acc}$ by applying the parametrization by Natta et al. (2004), that converts the Hα velocity wings at 10% of the maximum ($V_{H\alpha10\%}$) into $\dot{M}_{acc}$:

$$\dot{M}_{acc}/\mathrm{M}_\odot\,\mathrm{yr}^{-1} = -12.89 + 9.7\times10^{-3}V_{H\alpha10\%}\ , \tag{3}$$

In our high-resolution spectra $V_{H\alpha10\%}$ ranges between 550 and 630 km s^{-1}. From Equation 3 we derive the values of $\dot{M}_{acc}$ depicted with green points in Figure 7. Noticelably, they agree fairly well with those derived by us with the Alcalá et al. method. The only exception is the estimate derived from the spectrum of

Table 4. Parameters of the main Gaussians fitting the Hα line.

Date	Blue			Red			P Cygni		
	Center	FWHM	EW	Center	FWHM	EW	Center	FWHM	EW
(yyyy mm dd)	(km s^{-1})	(km s^{-1}	(km)	km s^{-1})	(km s^{-1}	(km)	(km s^{-1})	(km s^{-1})	(km)
2017 11 30	-188	147	-113	60	230	-472	-	-	-
2017 12 04	-214	161	-143	55	247	-601	-	-	-
2017 12 05	-218	130	-101	57	232	-414	-	-	-
2018 01 02[a]	-231	108	-88	12/82	67/213	-85/-214	-	-	
2018 01 28	-230	162	-115	55	250	-412	-92	98	111
2018 01 29[a]	-215	130	-91	40/160	106/134	-140/-105	-97	56	31

Notes. [a] The red component was fitted with two Gaussians.

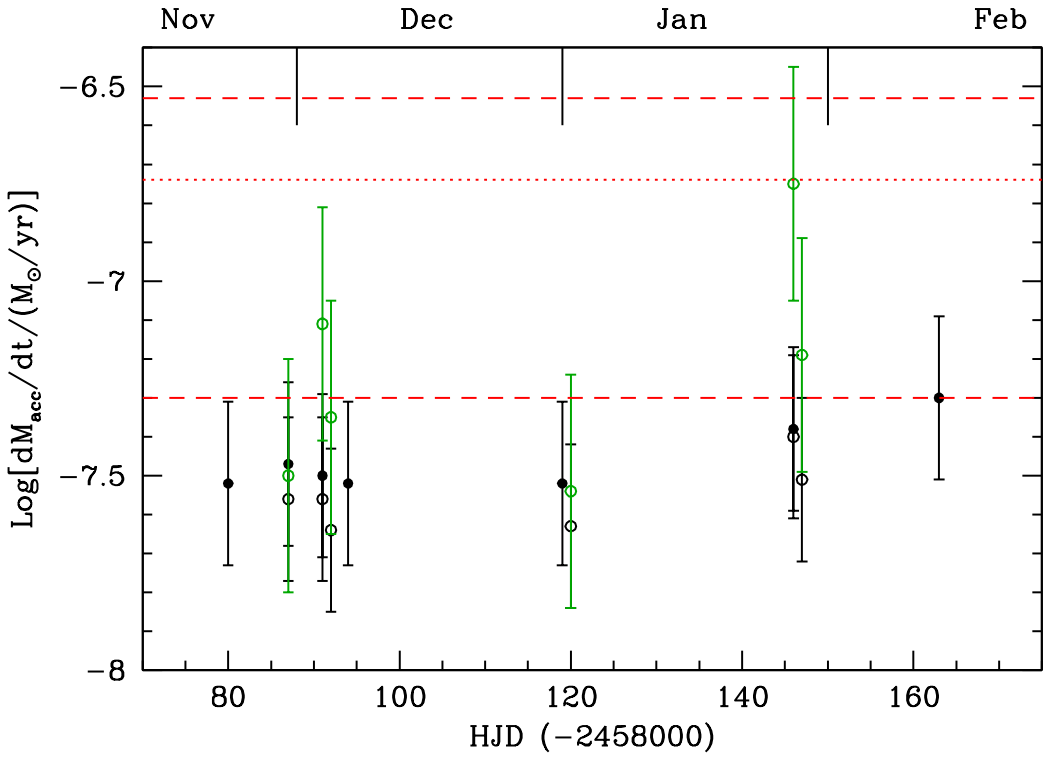

Fig. 7. Mass accretion rates derived from the Hα line flux in different dates. $\dot{M}_{acc}$ values derived from the relation by Alcalá et al. (2017) are depicted in black with filled and open symbols for low- and high-resolution spectra, respectively. Green data are the $\dot{M}_{acc}$ values derived with the method by Natta et al. (2004). In red is the comparison with literature determinations: dotted line is the value by Semkov et al. (2015), while the two dashed lines delimit the range found by Sicilia-Aguilar et al. (2008).

2018 Jan 28, where however the Hα profile likely suffers from self-absorption effects.

In conclusion, we can affirm that the mass accretion rate has remained substantially unchanged during our monitoring period. However, a bare correlation between source brightness and mass accretion rate can be recognized between epochs, such 2008 and 2017, in which the luminosity level is remarkably different.

4. Concluding remarks

Here, we shortly summarize the strong indications we have found that confirm the UXor nature of GM Cep:

- Optical two-colors and mag-color plots indicate how colors fluctuations are in very good agreement with the extinction vector. This is a necessary, but not sufficient condition to infer on the GM Cep nature.

- Archival plates do not contraddict the found condition.
- Low resolution spectra have roughly the same slope for different brightness conditions; they do not present other emission lines apart Hα, while Hβ is seen in absorption. Lines from neutral and ionized metals, have almost constant equivalent width at different dates, as expected in case of dust extinction fluctuations.
- Our simultaneous photometric and spectroscopic approach revealed as the real asset of this study: indeed it allowed us to conclude that the mass accretion rate remains fairly constant ($\sim 3.5 \times 10^{-8}$ $M_\odot\,yr^{-1}$) during the source brightness variations. All in all, GM Cep is a PMS object that naturally still accretes mass from its circumstellar disk, but in a quasi-steady way. Thus, mass accretion variations (if any) are not the main origin of the brightness fluctuations.

References

Alcalá, J. M., Manara, C. F., Natta, A., et al. 2017, A&A, 600, A20
Bibo, E. A., & The, P. S. 1990, A&A, 236, 155
Cardelli, J. A., Clayton, G. C., & Mathis, J. S. 1989, ApJ, 345, 245
Chen, W. P., Hu, S. C.-L., Errmann, R., et al. 2012, ApJ, 751, 118
Edwards, S., Fischer, W., Kwan, J., Hillenbrand, L., & Dupree, A. K. 2003, ApJ, 599, L41
Giannini, T., Munari, U., Antoniucci, S., et al. 2018, A&A, 611, A54
Grinin, V. P. 1988, Soviet Astronomy Letters, 14, 27
Grinin, V. P., Kozlova, O. V., Natta, A., et al. 2001, A&A, 379, 482
Grinin, V. P., The, P. S., de Winter, D., et al. 1994, A&A, 292, 165
Gullbring, E., Hartmann, L., Briceño, C., & Calvet, N. 1998, ApJ, 492, 323
Hartmann, L., Herczeg, G., & Calvet, N. 2016, ARA&A, 54, 135
Hartmann, L., & Kenyon, S. J. 1985, ApJ, 299, 462
Henden, A. A., Levine, S. E., Terrell, D., Smith, T. C., & Welch, D. 2012, Journal of the American Association of Variable Star Observers (JAAVSO), 40, 430
Henden, A., & Munari, U. 2014, Contributions of the Astronomical Observatory Skalnate
Herczeg, G. J., & Hillenbrand, L. A. 2008, ApJ, 681, 594-625
Herbig, G. H. 1989, European Southern Observatory Conference and Workshop Proceedings, 33, 233
Hillenbrand, L. A., Miller, A. A., Covey, K. R., et al. 2013, AJ, 145, 59
Huang, P.-C., Chen, W.-P., Hu, C.-L., et al. 2018, Bulletin de la Societè Royale des Sciences de Liége, 87
Jurdana-Šepić, R., Munari, U., Antoniucci, S., et al. 2017, A&A, 602, A99
Jurdana-Šepić, R., Munari, U., Antoniucci, S., Giannini, T., & Lorenzetti, D. 2018, arXiv:1801.10054
Kóspál, Á., Ábrahám, P., Acosta-Pulido, J. A., et al. 2016, A&A, 596, A52
Kun, M., Szegedi-Elek, E., Moór, A., et al. 2011, MNRAS, 413, 2689
Munari, U., Castellani, F., Giannini, T., Antoniucci, S., & Lorenzetti, D. 2017, The Astronomer's Telegram, 11004
Munari, U., Henden, A., Frigo, A., et al. 2014, AJ, 148, 81
Muzerolle, J., Calvet, N., & Hartmann, L. 2001, ApJ, 550, 944
Natta, A., Testi, L., Muzerolle, J., et al. 2004, A&A, 424, 603
Rigliaco, E., Natta, A., Testi, L., et al. 2012, A&A, 548, A56
Semkov, E. H., Ibryamov, S. I., Peneva, S. P., et al. 2015, PASA, 32, e011
Semkov, E. H., & Peneva, S. P. 2012, Ap&SS, 338, 95
Sicilia-Aguilar, A., Merín, B., Hormuth, F., et al. 2008, ApJ, 673, 382-399
Sicilia-Aguilar, A., Roccatagliata, V., Getman, K., et al. 2015, A&A, 573, A19
Valenti, J. A., Basri, G., & Johns, C. M. 1993, AJ, 106, 2024
Xiao, L., Kroll, P., & Henden, A. A. 2010, AJ, 139, 1527